Article:
Angus, C., Frost-Schenk, J., Laird, A. M. orcid.org/0000-0003-0423-363X et al. (7 more authors) (2024) Ne 21 energy levels approaching the α -particle threshold. Physical Review C. 044323. ISSN 2469-9993

https://doi.org/10.1103/PhysRevC.109.044323

^{21}Ne energy levels approaching the α-particle threshold

C. Angus,[1,2] J. Frost-Schenk,[1,*] A. M. Laird,[1] P. Adsley,[3,4,5,6] R. Longland,[7,8] C. J. Barton,[1] C. Aa. Diget,[1] C. Marshall,[7,8] F. Portillo Chaves,[7,8] and K. Setoodehnia[7,8]

[1]*School of Physics, Engineering and Technology, University of York, York YO10 5DD, United Kingdom*
[2]*TRIUMF, 4004 Wesbrook Mall, Vancouver, British Columbia V6T 2A3, Canada*
[3]*Cyclotron Institute, Texas A&M University, College Station, Texas, Texas 77843, USA*
[4]*Department of Physics and Astronomy, Texas A&M University, College Station, Texas, Texas 77843, USA*
[5]*iThemba Laboratory for Accelerator Based Sciences, Somerset West 7129, South Africa*
[6]*School of Physics, University of the Witwatersrand, Johannesburg 2050, South Africa*
[7]*Department of Physics, North Carolina State University, Raleigh, North Carolina, North Carolina 27695-8202, USA*
[8]*Triangle Universities Nuclear Laboratory, Durham, North Carolina, North Carolina 27708-0308, USA*

(Received 24 October 2023; accepted 22 March 2024; published 22 April 2024)

Background: Nuclei around ^{20}Ne exhibit an interplay of different excitations caused by different aspects of nuclear structure, including single-particle and multiparticle configurations and collective rotations. One-nucleon transfer reactions selectively probe single-particle structures in these nuclei. These nuclei are also important to astrophysics, with a number of important reactions proceeding through this mass region.
Purpose: Energy levels approaching the α-particle threshold in ^{21}Ne are of importance to nuclear structure. The ^{20}Ne$(d, p)^{21}$Ne reaction was measured and the corresponding spectroscopic nuclear information was extracted.
Method: States in ^{21}Ne were populated using the ^{20}Ne$(d, p)^{21}$Ne reaction in forward kinematics. Protons were identified in the Triangle Universities Nuclear Laboratory (TUNL) Enge split-pole spectrograph and angular distributions were extracted. Spin-party assignments were made and neutron partial widths were determined based on distorted-wave Born approximation (DWBA) analysis.
Results: Several new energy levels were observed at energies of 7176, 7235, 7250, and 7337 keV, and spin-parities are reported which generally agree with previous results where literature was available. Spin and parity assignments are reported for several energy levels along with estimated neutron widths for those states above the neutron threshold ($S_n = 6761$ keV).
Conclusions: Results from this study are placed in context with a review of the available literature on all known states in this energy region of ^{21}Ne.

DOI: 10.1103/PhysRevC.109.044323

I. INTRODUCTION

The region of the nuclear chart around ^{20}Ne features an interplay between different degrees of freedom in nuclear excitation. The strongly deformed nucleus ^{20}Ne exhibits rotational excitations of its ground state and α-particle shape isomers at higher energies, probably related to 4p-4h excitations [1]. In the region around ^{20}Ne, weak-coupling especially of 4p systems with one-particle or one-hole structures has been observed [2–5]. For example, the mirror rotational bands built on the first $J^\pi = \frac{1}{2}^-$ states in ^{19}Ne and ^{19}F are well described as a $p_{\frac{1}{2}}$ neutron (proton) hole coupled to an α-particle excitation. More complex structures, such as the 5p-2h configuration of the $E_x = 4033$ keV state in ^{19}Ne [6], critical to the ^{15}O$(\alpha, \gamma)^{19}$Ne breakout reaction in x-ray bursts, have been observed with implications for various astrophysical systems.

This strong interplay of few-body with collective excitations makes this region of the nuclear chart difficult to tackle from a theoretical basis, requiring models which can treat excitations from the $1p$ shell[1] into the $2s1d$ region. Better nuclear data are valuable for disinguishing these different origins of nuclear excitation, especially those data which can investigate the microscopic structure of these nuclei using single-nucleon transfer reactions or data which are sensitive to the collective properties of nuclei in this region such as Coulomb excitation, for example Refs. [7,8], or lifetime measurements.

The nucleus discussed in this paper, ^{21}Ne, is also of importance for nuclear astrophysics. In an earlier publication

*Present address: Department of Physics and Astronomy, University College London, London WC1E 6BT, United Kingdom.

[1]We use the convention that all nodes including that at the origin are counted and so shells start at 1.

[9], we focused on states above the α threshold, at 7384 keV, relevant to the $^{17}\mathrm{O}(\alpha, n)^{20}\mathrm{Ne}$ and $^{17}\mathrm{O}(\alpha, \gamma)^{21}\mathrm{Ne}$ reactions, which influence the synthesis of the heavy elements through the *s* process in massive stars. In this context, the cluster configurations of α particles with the $^{17}\mathrm{O}$ core potentially enhance the $^{17}\mathrm{O}+\alpha$ reactions and may be compared to the $^{16}\mathrm{O}+\alpha$ cluster structures found in $^{20}\mathrm{Ne}$. In this paper we report on the states around and below the α threshold detailing the current understanding of these states and reporting the experimental results obtained using the Triangle Universities Nuclear Laboratory (TUNL) split-pole spectrograph [10].

II. EXPERIMENTAL TECHNIQUE

States in $^{21}\mathrm{Ne}$ were populated using the neutron stripping $^{20}\mathrm{Ne}(d, p)^{21}\mathrm{Ne}$ reaction at the Triangle Universities Nuclear Laboratory (TUNL). Deuterons produced in the direct extraction negative ion source were accelerated though the TUNL 10 MV FN tandem accelerator, resulting in a beam with an energy of 13.984(4) MeV. This beam energy was chosen to balance the presence of background contamination in the spectrum with the required stability of the accelerator at high terminal voltages. The accelerated beam was momentum analyzed through two consecutive 90° magnets, producing a beam on target with small energy spread. The beam intensity at the target location was monitored using an electron-suppressed beam stop.

The beam was focused to a 44-$\mu g/cm^2$ natural carbon foil implanted with $^{20}\mathrm{Ne}$ located at the target position of the split-pole spectrograph [11]. The initial atomic abundance ratio of neon/carbon was determined to be $4.3 \pm 0.3\%$ by performing a separate Rutherford Backscattering spectrometery (RBS) measurement, also at TUNL [12]. Target stoichiometry as a function of depth was modelled and fit to the RBS spectrum using the software package SIMNRA [13]. It was found that changing the layer contents by around 5% significantly degraded the quality of the fits and so an uncertainty of 5% in the neon content was adopted. The deuteron beam was periodically returned to achieve approximately 90% transmission through a 1-mm-diameter collimator at the target position to ensure that the same region of the target was used throughout the experiment. Furthermore, a set of feedback steering elements on the spectrograph beamline prevented any drift in the beam position.

Reaction products passed through a 0.54 ± 0.01 mSr aperture into the split-pole spectrograph. The small aperture was chosen to minimise variation in the differential cross section across the aperture. Particles that traversed the split-pole's field region were then detected by the focal-plane detector, which consisted of two position-sensitive sections, a ΔE gas proportional counter and a full-energy scintillator detector. Further information on the TUNL split-pole spectrograph and focal-plane detector can be found in Ref. [10]. The position resolution of the focal-plane detector corresponded to approximately 10 keV (FWHM) for the present experiment.

Measurement angles were chosen to maximize the distinction between transferred ℓ values and ensure a reaction described by surface effects (and thus the distorted-wave Born approximation). Data were collected at laboratory scattering angles of 10°, 15°, 20°, 25°, and 38°. Beam intensities on the target varied from 300 to 575 nA with beam intensities lower for the 10° data, between 70 and 95 nA, to reduce detector exposure to beam. At each angle, a measurement was also made using a natural carbon target for background characterisation, including the identification and characterisation of the 5.084-MeV $^{17}\mathrm{O}$ state, an anticipated source of background in the experiment. Between each angle, the spectrograph was placed at a laboratory scattering angle of 25° for elastic scattering measurements to monitor target degradation. After normalizing to the beam current, the total counts in the elastically scattered carbon peaks were extracted, and it was found that there was no statistically significant change in the abundance of carbon in the target over the course of the experiment. The integral of the $^{20}\mathrm{Ne}$ elastic peak was taken in ratio with beam on target during each elastic run, and used to account for target degradation.

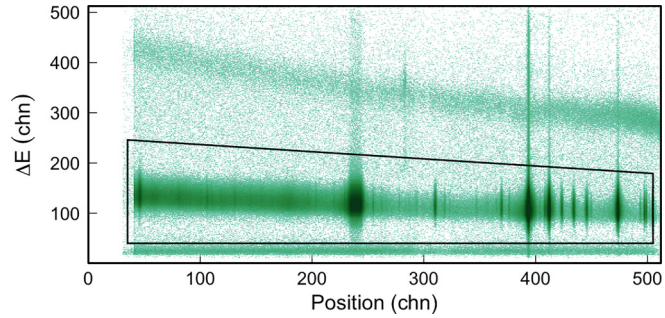

FIG. 1. Energy deposited in ΔE against front position on the focal plane detector for laboratory angle 20°.

III. DATA ANALYSIS

Utilizing the data acquisition software package JAM [14], gates were made based upon the ΔE and position, shown in Fig. 1. Two-dimensional (2D) cuts were chosen to remove deuterons, seen at higher ΔE component energy deposition, while removing minimal protons. Following this, additional 2D cuts were placed on the ΔE-E spectrum as shown in Fig. 2.

Having removed deuteron contamination, the spectra were internally calibrated. Initially, carbon peaks were identified

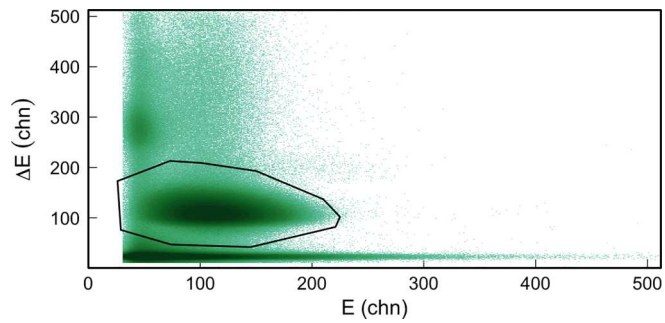

FIG. 2. Energy deposited in ΔE detector against energy deposited in E detector at a laboratory angle of 20°, ungated but with ΔE-E gate shown.

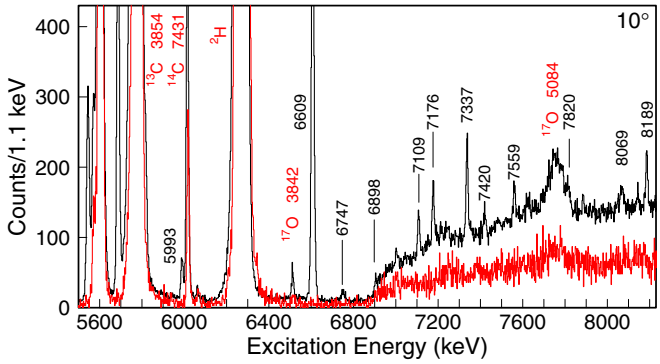

FIG. 3. Focal plane spectrum for protons at $\theta_{\text{lab}} = 10^{\circ}$. Red indicates the carbon spectrum.

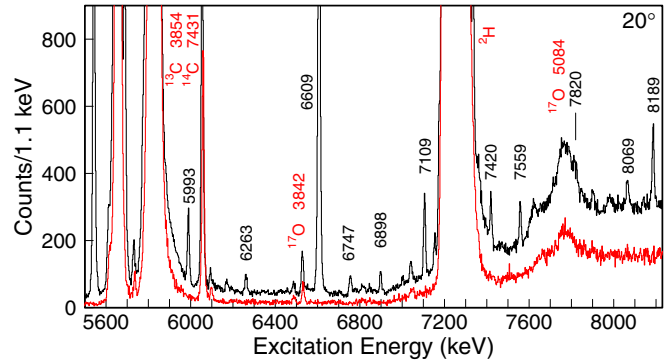

FIG. 5. Focal plane spectrum for protons at $\theta_{\text{lab}} = 20^{\circ}$. Red indicates the carbon spectrum.

corresponding to the ^{13}C excited states at $E_x = 3089$, 3685, and 3854 keV. These were then used to visually identify peaks corresponding to known ^{21}Ne states using kinematic predictions. For example, the 5334.4(10)- and 6609.0(10)-keV states as reported in Ref. [15] were trivially identified due to their intensities. Excitation energies were obtained by fitting the focal plane using a quadratic model and a Markov chain Monte Carlo method. This method is similar to that described in Ref. [10], and allows extraction of excitation energy uncertainties including intrinsic detector scatter coming from delay-line nonlinearity, calibration uncertainties, and channel uncertainties. Relativistic kinematics and target straggling effects were included. The states used for this internal calibration were 6609(1), 7420(1), 8069(2), and 8189(2) keV [15]. A weighted average was used to combine extracted energies over all measurement angles, but with final uncertainties conservatively constrained to be no smaller than the angle with the smallest measured uncertainty.

Figures 3–7 show the focal-pace excitation energy spectra for the fitted excitation-energy range of ^{21}Ne for angles of 10°, 15°, 20°, 25° and 38°, respectively. Note in the 25° data the substantial background from the $p(d, p)d$ reaction. Localized fits were made to subregions across the focal plane to better characterize and fit the background.

Differential cross sections were extracted for those states seen at multiple angles. Key sources of uncertainty in the differential cross sections included the target density, ∼7%, beam intensities, ∼7%, and the uncertainty on the number of protons, which was determined by the statistical uncertainties in the fit. Data acquisition dead time was accounted for using a 10 Hz clock signal.

The value of the spectroscopic factor, C^2S, was extracted by comparing the experimental differential cross section to the differential cross section calculated using the distorted-wave Born approximation (DWBA) using the code FRESCO [16]:

$$\frac{d\sigma}{d\Omega}_{\text{exp}} = C^2 S \frac{d\sigma}{d\Omega}_{\text{DWBA}} \tag{1}$$

An additional step in the analysis was needed to study energy levels above the neutron threshold (6761 keV in ^{21}Ne) using DWBA. Following the method described in Ref. [17], DWBA predictions for differential cross section were calculated at a series of energies below the neutron threshold to determine the trend of the predictions with energy. This trend was then used to scale the sub-threshold predictions for differential cross section to the desired excitation energy for each unbound state of interest. This step was necessary for analyzing the unbound states, since the form-factor integrals for states in the continuum do not converge, because the radial wave functions for such states decay too slowly with increasing radius.

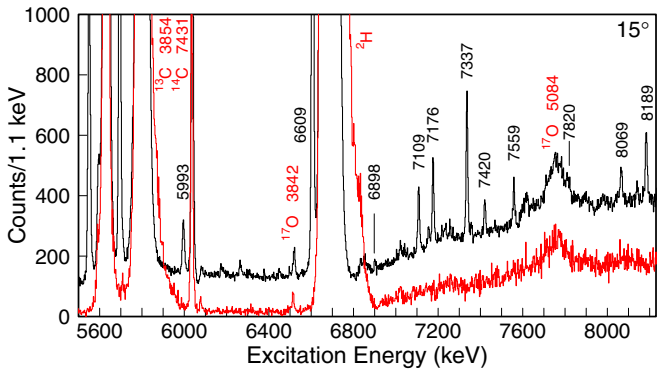

FIG. 4. Focal plane spectrum for protons at $\theta_{\text{lab}} = 15^{\circ}$. Red indicates the carbon spectrum.

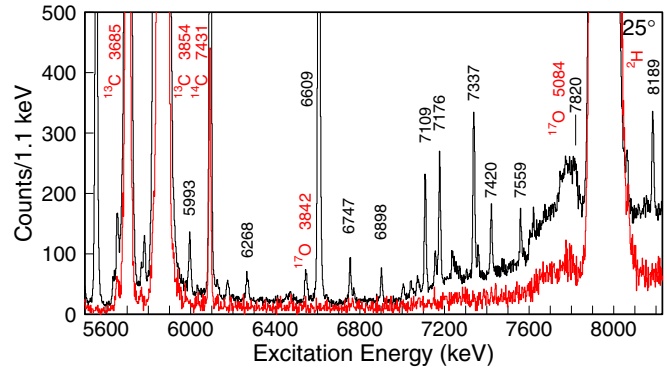

FIG. 6. Focal plane spectrum for protons at $\theta_{\text{lab}} = 25^{\circ}$. Note the contamination occurring from the $p(d, p)d$. Red indicates the carbon spectrum.

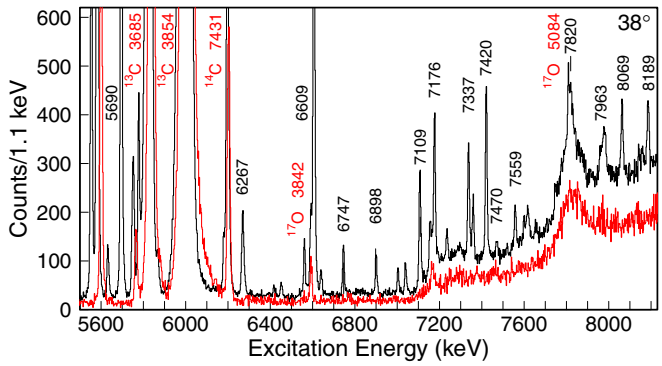

FIG. 7. Focal plane spectrum for protons at $\theta_{\rm lab} = 38^\circ$. Red indicates the carbon spectrum.

The global model potentials used in this analysis were from Ref. [18] for the ^{20}Ne + ^{2}H interaction and the Gaussian shaped potential from Ref. [19] for the $n + p$ interaction. The ^{20}Ne $+n$, ^{21}Ne $+p$, and ^{20}Ne $+p$ interactions are all calculated from Ref. [20]. The choice of global optical model potentials was made for consistency with Ref. [20]. The global nucleon potential described in Ref. [19] was based on data for nuclei $A = 40$–209. Since ^{20}Ne is below that mass range, it was desirable to explore the reliability of the DWBA predictions. Figure 8 shows a plot comparing the effects of varying the optical model parameters for the ^{20}Ne $+n$, ^{21}Ne $+p$, and ^{20}Ne $+p$ interactions by $\pm 10\%$, while maintaining a constant binding energy. As can be observed in Fig. 8, the DWBA predictions are similar under 30°, which is the angular range used for comparison with data.

The penetrability of the unbound states was calculated using Eq. 2.162 from Ref. [21]. The dimensionless single-particle reduce widths for each state were calculated from the single-particle wave functions computed by FRESCO [16]. Values for C^2S, $\theta^2_{\rm sp}$, P_ℓ, and neutron partial widths were be determined with Eq. 7 of Iliadis (1997) [22]. Just as in the C^2S determination, values for Γ_n were calculated at a series of

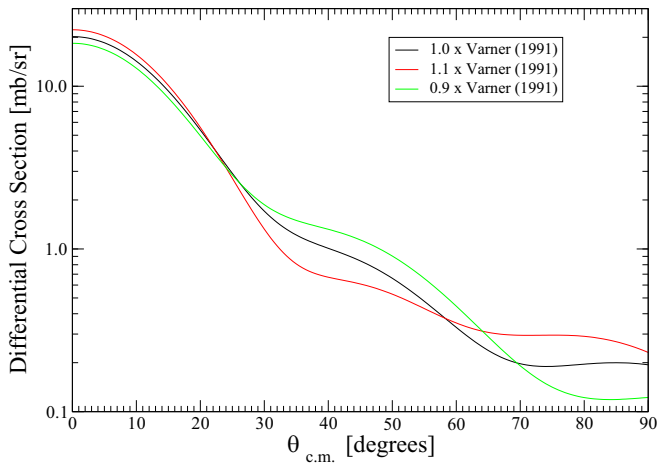

FIG. 8. A comparison of DWBA predictions for the 6609-keV state (assuming $2J^\pi = 3^-$), made by varying the global nucleon potential [20] by $\pm 10\%$.

energies below the neutron threshold to find their trend with energy, then extrapolated to the desired excitation energy. As in Ref. [9], partial widths were evaluated at radius a, where the ^{20}Ne $+n$ wave function is at 99% of the asymptotic value (see Refs. [23] for more details).

Where the measured width of a peak was greater than the detector resolution (approximately 10 keV), the fitting parameters were allowed to vary such that the average standard deviation of the fits could be extracted and used to calculate the width of that energy level. In such cases, the upper limits were set arbitrarily but always used the detector resolution as a lower limit. Where such measurements were available, they have been included in Table I.

Data were taken in this experiment at a number of angles, including 38°. Previous experimental data [24] show that, at higher angles, the calculated differential cross sections are significantly below the experimental data. Calculations using FRESCO were performed including the possibility of inelastic excitation of the strongly deformed ^{20}Ne target followed by transfer from this state as well as single-step direct transfer from the ground state of ^{20}Ne. These calculations were in good agreement at smaller angles with calculations describing only the single-step direct transfer from the ground state but were markedly different at higher angles. For this reason, the 38° data were excluded from the DWBA analysis. The data are still valuable for determining the excitation energies of ^{21}Ne levels.

IV. RESULTS AND DISCUSSION

Table I contains the results from this study. Spin-parities are reported only for states that are observed at at least three angles below 38°. The rest were observed at at least two angles (including 38°) and their energies are reported. A brief summary of each state in this region can be found in Table I, including the results from this study. In the following sections, the available literature on the ^{21}Ne states is summarized and comparisons with the present results are made. Plots compare different ℓ transfers, choosing only one of the possible J^π values for clarity, since this analysis cannot distinguish between different J^π's of the same ℓ transfer. In general, (d, p) reactions struggle to discriminate between different transfers with the same L and different $J = L \pm \frac{1}{2}$. There is some evidence in the literature that this is possible with measurements at higher angles [27,28], but these effects are small and probably confounded in the current experiment due to the strong effect of the deformation of the ^{20}Ne target, coupling through which tends to change the cross section at higher angles significantly.

5994 keV: This state was observed in this study and the measured excitation energy of 5994(3) keV is in agreement with the compilation value of 5992.56(8) keV [25]. The best fitting angular distribution prediction, as seen in Fig. 9, was $\ell = 1$, agreeing with the literature spin-parity of $J^\pi = \frac{3}{2}^-$ which was determined by Ref. [29] in a ^{22}Ne$(d,t)^{21}$Ne reaction study. It should be noted that ^{22}Ne$(d,t)^{21}$Ne study often displayed poor agreement between DWBA predictions and measured data. Through analysis of an ^{18}O$(\alpha, n\gamma)^{21}$Ne

TABLE I. A list of the energy levels observed in this study and a comparison to literature energies. Deduced spin-parities from this study and from literature are also included where possible. The neutron separation energy of 6761.16 keV is marked by a line between rows. Where a state has two possibilities for spin-parity, the results are listed with the smaller J value first; the options for C^2S and Γ_n values are listed in the same order as their associated J^π.

E_x (keV)				$2J^\pi$		Γ_n(eV)	
This work	Literature[a]	C^2S	ℓ_n	This work	Literature[a]	This work	Literature[a]
5994(3)	5992.56(8)	0.014, 0.024	1	$(1, 3)^-$	3^-		
	6033.3(3)				9^-		
6096(3)[b]							
6175(3)	6174.2(17)				$(5)^+$		
	6263(2)				(7^+)		
6268(2)	6267.0(16)				9^+		
	6412.5(13)				7^+[c]		
	6448.3(10)				(13^+)		
	6543.5(10)				9^+[b]		
6549(1)	6554.2(7)				9		
6609(2)	6609.0(10)	0.102, 0.122	2	$(3, 5)^+$	$(3, 5)^+$		
	6640.7(10)				$9^{(-)}$		
6753(2)	6748.5(15)	0.008, 0.014	3	$(5, 7)^-$			
	6761.11(3)						
	6853(20)						
6901(1)	6901.16(4)				1^-	1120(160), 630(90)	861(29)
7004(2)	7008.7(23)				7^+		
	7022.8(13)				(7^+)		
7041(1)	7043.9(11)				$(9)^+$		
7108(1)	7109(4)	0.104, 0.120	2	$(3, 5)^+$		160(20), 120(10)	
		or	or	or		or	
		0.145, 0.132	3	$(5, 7)^-$		2.9(2), 2.5(2)	
7156(1)	7154(5)						
7176(1)		0.129, 0.118	2	$(3, 5)^+$		300(20), 220(20)	
	7211.1(5)				1^+		107 800(1100)
7218(2)	7226(5)						
7235(1)							
7250(2)							
	7294(20)						
	7320(5)				(1^+)		
7337(1)		0.167, 0.140	2	$(3, 5)^+$		960(50), 960(80)	
7357(2)	7362.7(15)				$(7^+, 9^+)$		
	7370.6(17)				(7^-)		

[a]NNDC [25] unless otherwise noted.
[b]Possible observation.
[c]Proposed in Ref. [26] but not recorded in NNDC [25].

experiment, Ref. [30] limited the lifetime of this state to <10 fs.

6033.3 keV: The spin-parity for this state was assigned by Ref. [31] using a ^{18}O$(\alpha, n\gamma)^{21}$Ne experiment, with which the studies of Refs. [32] and [26] are in agreement. The most precise reported lifetime is 19(2) fs, measured by Ref. [33] in an ^{12}C$(^{13}$C$, \alpha\gamma)^{21}$Ne experiment. Despite being observed in past ^{20}Ne$(d, p)^{21}$Ne reactions [24] this state was not observed in this study. A small peak in the 15° spectrum could indicate its presence; however, this was the only angle for which a level at this energy was observed and, without a second observation at different angle, it was not possible to confirm that this was not a background artifact. At 10° it is likely underneath the background, and while several unidentified peaks appear in this region on the 20° and 25° spectra, none are within uncertainty of the expected energy. It is possible that the high spin-parity expected from Ref. [31] meant that this state was not strongly enough populated by a (d, p) reaction for it to be reliably observed in this work.

6096 keV: No state has previously been reported at this energy; however, a peak was measured on the proton spectrum at two angles (20° and 25°) within 1 keV. The corresponding differential cross section at these two angles drops by one order of magnitude over 5°, a magnitude not observed in any of the other energy levels investigated. Furthermore, since this state was only observed at these two angles, it is possible that it originated from the background, and therefore this state is reported here as a possible observation only.

6175 keV: This state has been observed in many previous studies using various reactions (including (d,p) experiments

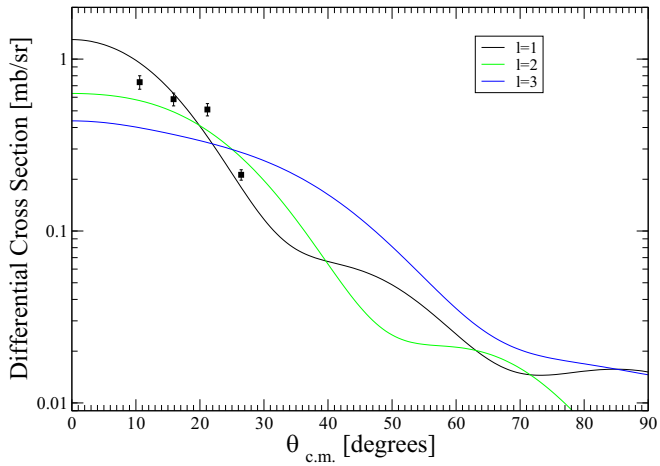

FIG. 9. The differential cross section of the $E_x = 5.994$ MeV state populated in the ^{20}Ne$(d, p)^{21}$Ne reaction. The displayed curves are (black) $\ell = 1$ to populate a $J^\pi = \frac{3}{2}^-$ state, with $\chi^2 = 27.18$, (green) $\ell = 2$ to populate a $J^\pi = \frac{5}{2}^+$ state, with $\chi^2 = 33.58$, and (blue) $\ell = 3$ to populate a $J^\pi = \frac{7}{2}^-$ state, with $\chi^2 = 92.56$. The best fit for this energy level was $\ell = 1$.

[24]). The literature spin-parity was determined to be $J^\pi = \frac{5}{2}^+$ in an ^{16}O$(^7$Li$, np\gamma)^{21}$Ne experiment [26]. Reference [34] reported the lifetime of this state in an ^{18}O$(\alpha, n\gamma)^{21}$Ne experiment as 35(18) fs, in mild tension with the results of Ref. [33], which determined the lifetime to be 13(6) fs. This state was observed in this experiment at angles of 20° and 25°.

6263 keV: This state has been observed in three previous experiments: a ^{12}C$(^{13}$C$, \alpha\gamma)^{21}$Ne study by Ref. [35] and in two ^{16}O$(^7$Li$, np\gamma)^{21}$Ne studies by Refs. [26] and [32], that all agree with a spin-parity assignment of $J^\pi = \frac{7}{2}^+$. A peak at the correct energy was observed at 20° and may belong to this state; however, without a second observation, it cannot be reliably identified in these data. A spin-parity of $J^\pi = \frac{7}{2}^+$ would produce an $\ell = 4$ transfer in a (d, p) reaction. High-spin states such as 6263 keV were not strongly populated in this experiment, given the low angular momentum of the projectile (deuteron) and ejectile (proton). This could be the reason why this state was not reliably observed in this study.

6268 keV: The literature spin-parity for this state was determined to be $J^\pi = \frac{9}{2}^+$ by two separate experiments: Ref. [31] with an ^{18}O$(\alpha, n\gamma)^{21}$Ne experiment and Ref. [26] with an ^{16}O$(^7$Li$, np\gamma)^{21}$Ne experiment. Results from another ^{18}O$(\alpha, n\gamma)^{21}$Ne experiment by Ref. [36], conducted prior to Ref. [31], indicated a spin of either $J = \frac{9}{2}$ or (less likely) $J = \frac{7}{2}$. Interestingly, Ref. [33] favored the assignment of $J^\pi = \frac{7}{2}^+$ based on an analysis of the intensities of γ rays from their ^{12}C$(^{13}$C$, \alpha\gamma)^{21}$Ne experiment. Reference [33] also measured the lifetime of this state as being <20 fs, which agrees with a previous ^{18}O$(\alpha, n\gamma)^{21}$Ne measurement by Ref. [30]. Another lifetime measurement of 35(18) fs was made by Ref. [34] though the large uncertainty means that there is some overlap between that result and previous measurements. This state was observed in this experiment at angles of 25° and 38° and so no spin-parity could be determined for this state.

6412.5 keV: This state has been observed in two previous ^{16}O$(^7$Li$, np\gamma)^{21}$Ne experiments [26,32]. Reference [26] proposed a spin-parity of $J^\pi = \frac{7}{2}^+$. Such a high spin-parity could explain why this state was not observed in this study.

6448.3 keV: This state has been observed in several previous experiments using a variety of methods, significantly in a previous (d, p) study [24]. The literature spin-parity assignment for this state is from the ^{18}O$(\alpha, n\gamma)^{21}$Ne experiment by Ref. [31] and the lifetime measurement of <20 fs is from an ^{12}C$(^{13}$C$, \alpha\gamma)^{21}$Ne experiment [33]. No level was observed at this energy in this experiment, as can be seen on Figs. 5 and 6.

6543.5 keV: This state was reported in the ^{16}O$(^7$Li$, np\gamma)^{21}$Ne studies of Refs. [32] and [26], with both experiments agreeing on a $J = \frac{9}{2}$ assignment and Ref. [26] additionally proposing a positive parity. No state was observed at this energy in this experiment.

6549 keV: A state was observed at this energy in this study and is likely to be the state reported in compilations as 6554.2(7) keV [15,25] and in Ref. [37] as 6551.7(10) keV. The literature spin-parity of $\frac{9}{2}$ comes from a ^{18}O$(\alpha, n\gamma)^{21}$Ne experiment [31]. Ref. [33] constrained the lifetime of this state to being <21 fs in a ^{12}C$(^{13}$C$, \alpha\gamma)^{21}$Ne experiment. Before that, Ref. [30] had reported the lifetime of this state as being 45(30) fs based on results from their ^{18}O$(\alpha, n\gamma)^{21}$Ne experiment, and Ref. [34] found it to be <35 fs. Regrettably, in this study the 6549(1) keV state was only observed at angles of 20° and 25° and thus could not be used to estimate the spin-parity.

6609 keV: This is a very prominent energy level on the proton spectrum of ^{20}Ne$(d, p)^{21}$Ne experiments [24,38], as is the case here. Reference [30] constrained the lifetime of this state to <10 fs in an ^{18}O$(\alpha, n\gamma)^{21}$Ne experiment. Previous studies found a best fitting spin-parity of $J^\pi = \frac{3}{2}^+$ or $\frac{5}{2}^+$ [38], implying an $\ell = 2$ transfer with which this study is in agreement, as can be seen in Fig. 10.

6640.7 keV: This state has been measured several times before and has an excitation energy of 6640.7(10) keV in Ref. [25]. The spin-parity is recorded as $\frac{9}{2}^{(-)}$ with Ref. [31] reporting the $\frac{9}{2}$ and Ref. [26] tentatively adding a negative parity. This state was not observed in this experiment; again, this is likely due to high spin-parity states not being strongly populated in (d, p) experiments.

6753 keV: Reference [33] reported the excitation energy for this state as 6748.5(15) keV and Ref. [31] as 6737(2) keV in a ^{12}C$(^{13}$C$, \alpha\gamma)^{21}$Ne study and an ^{18}O$(\alpha, n\gamma)^{21}$Ne study respectively. Reference [33] determined the lifetime as being 14(5) fs. No value for spin-parity has previously been reported. In this experiment this state was measured at an excitation energy which disagrees with the two other studies. On the 38° spectrum, this energy level was measured at 6747 keV whereas the other three observations (10°, 15°, and 25°) all measured it around 6755 keV. Since these differences in energy are significant and the energy calibrations were otherwise in good agreement with literature across the spectra, it is possible that there are several different levels close to one another in energy being observed in this region that dominate the fit at different angles of measurement. The differential cross

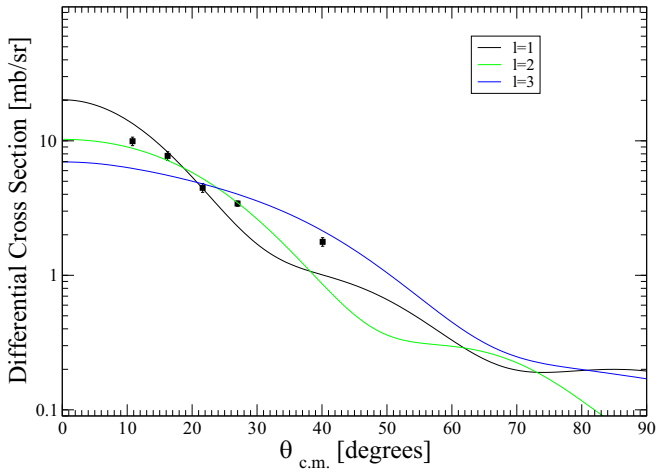

FIG. 10. The differential cross section of the $E_x = 6.609$-MeV populated in the ^{20}Ne$(d, p)\,^{21}$Ne reaction. The displayed curves are (black) $\ell = 1$ to populate a $J^\pi = \frac{3}{2}^-$ state, with $\chi^2 = 99.11$, (green) $\ell = 2$ to populate a $J^\pi = \frac{5}{2}^+$ state, with $\chi^2 = 11.64$, and (blue) $\ell = 3$ to populate a $J^\pi = \frac{7}{2}^-$ state, with $\chi^2 = 46.78$. The best fit for this energy level was $\ell = 2$. The 38° data point has been included in this plot but was not used in DWBA analysis.

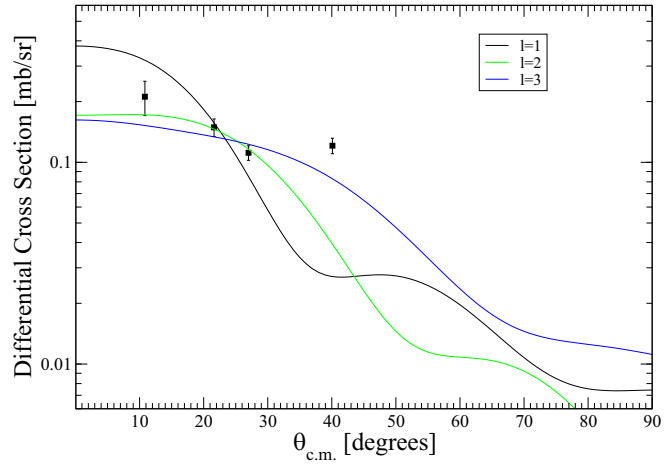

FIG. 12. The differential cross section of the $E_x = 6.901$ MeV state populated in the ^{20}Ne$(d, p)\,^{21}$Ne reaction. The displayed curves are (black) $\ell = 1$ to populate a $J^\pi = \frac{3}{2}^-$ state, with $\chi^2 = 15.08$, (green) $\ell = 2$ to populate a $J^\pi = \frac{5}{2}^+$ state, with $\chi^2 = 1.27$, and (blue) $\ell = 3$ to populate a $J^\pi = \frac{7}{2}^-$ state, with $\chi^2 = 4.79$. The best fit for this energy level was $\ell = 2$. The 38° data point has been included in this plot but was not used in DWBA analysis.

section measured in this study best fits a transfer of $\ell = 3$, which results in a spin-parity assignment of $J^\pi = \frac{5}{2}^-$ or $\frac{7}{2}^-$. A comparison of these data with different possible ℓ transfers is shown in Fig. 11. Since the ℓ transfer is deduced without the 38° point, this result would apply to the higher energy peaks grouped around 6755 keV, if indeed there are two separate states here.

6761.11 keV: This state has been measured in neutron capture experiments such as Ref. [39], which placed the excitation energy at 6761.16(4) keV. Reference [40] placed the excitation energy at 6760.8(15) keV and simultaneously measured the γ-ray spectrum of ^{21}Ne. This state was not observed in this study, indicating that this state has a small spectroscopic factor, or that it has a high spin-parity.

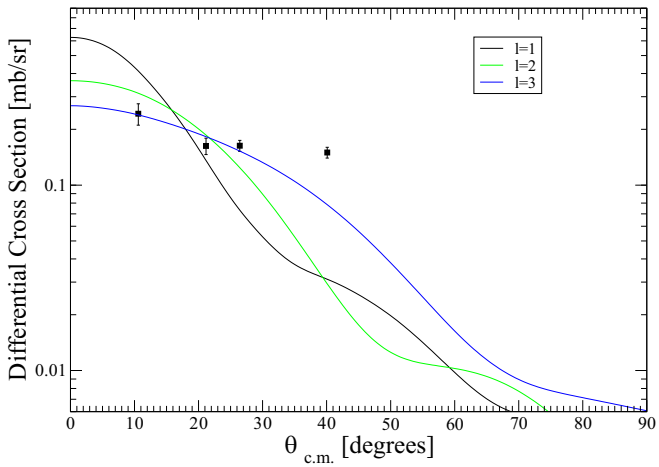

FIG. 11. The differential cross section of the $E_x = 6.753$ MeV state populated in the ^{20}Ne$(d, p)\,^{21}$Ne reaction. The displayed curves are (black) $\ell = 1$ to populate a $J^\pi = \frac{3}{2}^-$ state, with $\chi^2 = 95.05$, (green) $\ell = 2$ to populate a $J^\pi = \frac{5}{2}^+$ state, with $\chi^2 = 19.94$, and (blue) $\ell = 3$ to populate a $J^\pi = \frac{7}{2}^-$ state, with $\chi^2 = 2.54$. The best fit for this energy level was $\ell = 3$. The 38° data point has been included in this plot but was not used in DWBA analysis.

6853 keV: This state has so far only been measured by Ref. [41] at an energy of 6853(20) keV with a ^{19}F$(^3$He, $p)\,^{21}$Ne reaction. It was also included by Ref. [24] in the fit of their ^{20}Ne$(d, p)\,^{21}$Ne reaction spectrum but no spin-parity was reported, since the state appeared to have a small spectroscopic factor in that study. A small spectroscopic factor is a possible reason why this state was not observed in this experiment.

6901 keV: Previous experiments assigned this state's spin-parity as $J^\pi = \frac{1}{2}^-$ [29] through a ^{22}Ne$(d, t)\,^{21}$Ne experiment. It should be noted that the ^{22}Ne$(d, t)\,^{21}$Ne study displayed significant variation between the best fitting DWBA predictions and the experimental data. The literature γ-ray and neutron widths were determined in a ^{20}Ne$(n, \gamma)\,^{21}$Ne experiment as $\Gamma_\gamma = 3.7(2)$ eV and $\Gamma_n = 861(29)$ eV respectively [42]. That study, however, disagreed with another resonance neutron capture study which reported a significantly smaller neutron width [43]. This state was observed in this study. However, it appeared on the 10° spectrum on the edge of a background feature; the choice of different background function used when fitting the spectrum resulted in different ℓ transfers best fitting the data, and none of the background functions could be justified over the others. Therefore, due to an inability to properly control the background, the ℓ transfer for this state could not be reliably deduced. Figure 12 shows the resulting angular distribution when assuming a linear background function for the 10° spectrum fit of this state. Despite no result for the spin-parity, it was decided that these data would be used to calculate a neutron width and confirm agreement with

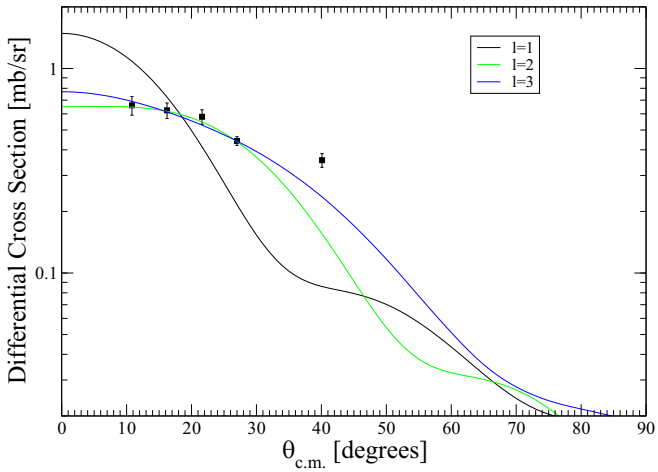

FIG. 13. The differential cross section of the $E_x = 7.108$ MeV state populated in the ^{20}Ne$(d, p)^{21}$Ne reaction. The displayed curves are (black) $\ell = 1$ to populate a $J^\pi = \frac{3}{2}^-$ state, with $\chi^2 = 130.90$, (green) $\ell = 2$ to populate a $J^\pi = \frac{5}{2}^+$ state, with $\chi^2 = 0.9$, and (blue) $\ell = 3$ to populate a $J^\pi = \frac{7}{2}^-$ state, with $\chi^2 = 1.42$. The best fit for this energy level was either $\ell = 2$ or $\ell = 3$, which could not be discriminated between. The 38° data point has been included in this plot but was not used in DWBA analysis.

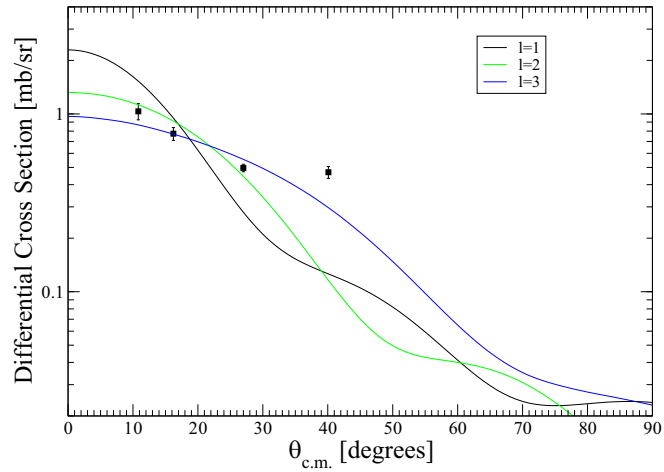

FIG. 14. The differential cross section of the $E_x = 7.176$ MeV state populated in the ^{20}Ne$(d, p)^{21}$Ne reaction. The displayed curves are (black) $\ell = 1$ to populate a $J^\pi = \frac{3}{2}^-$ state, with $\chi^2 = 82.02$, (green) $\ell = 2$ to populate a $J^\pi = \frac{5}{2}^+$ state, with $\chi^2 = 9.67$, and (blue) $\ell = 3$ to populate a $J^\pi = \frac{7}{2}^-$ state, with $\chi^2 = 5.79$. The best fit for this energy level was $\ell = 2$. The 38° data point has been included in this plot but was not used in DWBA analysis.

literature. When assuming a literature spin-parity of $\ell = 1$, these data yielded a neutron width of $\Gamma_n = 1120(160)$ eV or $\Gamma_n = 630(90)$ eV for $J^\pi = \frac{1}{2}^-$ or $J^\pi = \frac{3}{2}^-$ respectively, similar to previous results.

7004 keV: The literature value for the J^π of this state is $\frac{7}{2}^+$ and comes from an ^{18}O$(\alpha, n\gamma)^{21}$Ne experiment [31]. The lifetime measurement of <17 fs for this state came from Ref. [33]. This state was observed in this experiment at angles of 10°, 25°, and 38°. As only the two lower states could be used for DWBA analysis, this was not enough to reliably determine a spin-parity.

7022.8 keV: The energy of state was reported by Ref. [35] as $E_x = 7030(10)$ keV in a ^{12}C$(^{13}$C$, \alpha)^{21}$Ne reaction and again by Ref. [32] in an ^{16}O$(^7$Li$, np\gamma)^{21}$Ne reaction. The spin-parity assignment of $\frac{7}{2}^+$ is given in the compilations [15,25] and comes from Ref. [32]. It was assigned on the basis that opposite parity structures are connected by strong dipole transitions. This was, however, a tentative assignment and so should be reported as $(\frac{7}{2}^+)$. No state was observed at this excitation energy in this experiment, possibly due to the high expected spin-parity.

7041 keV: Literature compilations tentatively report the spin-parity for this state as $J^\pi = \frac{9}{2}^+$ [31,32]. Reference [33] measured the lifetime of this state as being 19(4) fs. This state was observed in this experiment at angles of 38°, 25°, and 20°, thus it was not assigned a spin-parity.

7108 keV: The 7108-keV state has only been observed twice prior to this experiment, by Ref. [41] in a ^{19}F$(^3$He$, p)^{21}$Ne study and by Ref. [34] in an ^{18}O$(\alpha, n\gamma)^{21}$Ne experiment. However, no spin-parities were reported. This state was observed in this study and it was found to fit both $\ell = 2$ and $\ell = 3$, as shown in Fig. 13. The low statistics of the data means that χ^2 values from the fitting could not be used to distinguish between $\ell = 2$ and $\ell = 3$.

7156 keV: This state has been observed in at least three previous experiments. However, no spin-parity has previously been reported [34,35,41]. The spectra in Figs. 5–7 show that this peak was difficult to discern in these data due to a ^{14}N contaminant present in the target, nevertheless it was observed at angles 38°, 25°, and 15°. Given that the 38° point is not used in DWBA fitting, there were insufficient data points to produce a reliable spin-parity.

7176 keV: This state has not been previously reported, but forms a quite prominent peak in the proton energy spectra in this experiment. That the excitation energy did not vary significantly from angle to angle in this study implies that this is not a contaminant peak intruding on the spectrum but is in fact an energy level in ^{21}Ne. The spin-parity deduced from these data best matches DWBA predictions for an $\ell = 2$ transfer, implying a J^π of either $\frac{3}{2}^+$ or $\frac{5}{2}^+$. A comparison of these data with different possible ℓ transfers is shown in Fig. 14.

7211.1 keV: This state was reported by Ref. [42], which used a neutron resonance scattering experiment to assign the spin-parity as being $\frac{1}{2}^+$ and the total width as 107.8 ± 1.1 keV. The positive parity assignment disagreed with that previously reported by Ref. [29] although both papers agree that the J value was $\frac{1}{2}$. Ref. [29] used a ^{22}Ne(d, t) reaction and also measured the width as being large (107 ± 6 keV). However, that analysis displayed significant variation between predicted and measured differential cross sections. This state was not observed in this study, possibly due to the relatively large width making it difficult to identify above background.

7218 keV: While observed in this study, this state was only measured at angles of 15° and 10°, so no spin-parity assignment could be made. This state is close in energy to a state previously reported in literature at 7226(5) keV [34,41].

Since no state was observed in this study at 7226 keV, it is likely that the 7218(2) keV observations belong to the same state.

7235 keV: This state is not reported in the compilations [15,25,37]. However, the state was observed in the present study at angles of 38°, 25°, and 15°. Though close in energy, this state is not the 7226(5) keV state reported in literature since both peaks were simultaneously observed on the 15° spectrum, with the 7226(5) keV state being measured at the lower energy of 7218(2) keV.

7250 keV: This state is not recorded in the literature compilations [15,25,37]. It was observed in this study at angles of 15° and 10°. A spin-parity assignment could not be made with these data.

7294 keV: This was not observed in this experiment and has only been reported once before at 7290(20) keV by Ref. [41]. Due to the systematic error in that paper, the value included in Ref. [37] was reevaluated as 7294(20) keV. Since this state was in a region of the focal plane relatively clear of background, it is likely that the reason for this state not being observed here is that is has a small spectroscopic factor and/or a high spin.

7320 keV: The excitation energy of 7320(5) keV was reported in Ref. [34] in an ^{18}O$(\alpha, n\gamma)^{21}$Ne study. Ref. [44] identified the J^π as $\frac{1}{2}^+$ with a ^{12}C$(^{13}$C, ^{21}Ne$)^4$He experiment. This state was not observed in this experiment, despite the expected low spin-parity, which should have meant that this state would be populated in this study. Since the background in this region is clear for most spectra, the likely reason for not having observed this state is that it has a small spectroscopic factor.

7337 keV: This is a newly reported energy level since, with an uncertainty of 1 keV, it is significantly separated from its nearest known neighbor at 7320(5) keV. Previously, Ref. [41] observed an energy level at 7326(10) keV, which is usually treated in compilations as a measurement of the 7320-keV state; however, that ^{19}F$(^3$He, $p\gamma)^{21}$Ne experiment suffered from a systematic error that lowered the measured energies [37]. Therefore, their measurement is likely higher than the value reported in the original paper, meaning that that study may have in fact been measuring this state. These data best fit an $\ell = 2$ transfer, as shown in Fig. 15, therefore the spin-parity assignment is $\frac{3}{2}^+$ or $\frac{5}{2}^+$.

7357 keV: This state has been reported several times previously with various reactions. The spin-parity assignment of $(\frac{7}{2}^+, \frac{9}{2}^+)$ in the compilations [15,25,37] originates from the ^{18}O$(\alpha, n\gamma)^{21}$Ne experiment of Ref. [31]. The ^{12}C$(^{12}$C, ^{4}He$)^{21}$Ne experiment by Ref. [44] agrees with this assignment. Reference [33] constrained the lifetime as being <11 fs. This state was observed in this study at angles of 15° and 25°.

7370.6 keV: This state has only been reported once: at 7370.6(17) keV in an ^{16}O$(^7$Li, $np\gamma)^{21}$Ne experiment [26]. That work notes that the energy is significantly different from the nearest other state (7357 keV). The spin-parity tentatively assigned by Ref. [26] was $J^\pi = \frac{7}{2}^-$ which has a different parity than the assignments for the $E_x = 7357$ keV state. The only other paper to report a state at this energy was Ref. [34], which measured a state at 7375(5) keV. This is usually recorded as a measurement of the lower 7357-keV state, which has been seen in other ^{18}O$(\alpha, n\gamma)^{21}$Ne reactions [31]. This state was not observed in this experiment, suggesting that the spectroscopic factor for this state is small.

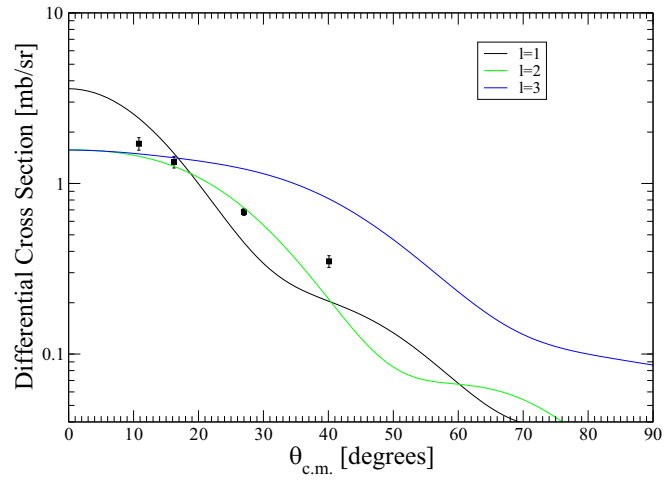

FIG. 15. The differential cross section of the $E_x = 7.337$ MeV state populated in the ^{20}Ne$(d, p)^{21}$Ne reaction. The displayed curves are (black) $\ell = 1$ to populate a $J^\pi = \frac{3}{2}^-$ state, with $\chi^2 = 77.27$, (green) $\ell = 2$ to populate a $J^\pi = \frac{5}{2}^+$ state, with $\chi^2 = 5.37$, (blue) $\ell = 3$ to populate a $J^\pi = \frac{7}{2}^-$ state, with $\chi^2 = 53.45$. The best fit for this energy level was $\ell = 2$. The 38° data point has been included in this plot but was not used in DWBA analysis.

V. SUMMARY

Despite being stable, the level structure for ^{21}Ne is relatively incomplete. The neon isotopes lie at a region of the nuclear chart with strong interplay between deformation, clustering, and few-particle modes of excitation, and are an important testing ground for structural models incorporating all of these aspects. Here, the ^{20}Ne$(d, p)^{21}$Ne reaction in forward kinematics was used to study the energy levels of ^{21}Ne. This paper follows Ref. [9], which investigated energy levels relevant for *s*-process nucleosynthesis. Here, results for those lower energy levels not investigated in the previous work have been presented following DWBA analysis. Agreement has been established with literature for the well known, strongly populated peaks below the neutron threshold, although there is some disagreement with the spin-parity assignments for higher energy levels. Spin-parities were calculated for the energy levels at 6753, 710, 7176, and 7377 keV, for which no spin-parities had previously been reported. Neutron widths were also calculated for those states above the neutron threshold. In addition to these results, a review of the available literature for those states between the neutron and α thresholds was conducted and has been summarized here.

ACKNOWLEDGMENTS

C.A., J.F.-S., A.M.L., C.J.B., and C.A.D. wish to acknowledge the support of the UK Science and Technology Facilities

Council (STFC). P.A. thanks the trustees and staff of Claude Leon Foundation for support in the form of a postdoctoral fellowship. R.L., C.M., F.P.C., and K.S. thank the U.S. Department of Energy, Office of Science, Office of Nuclear Physics, for support under Award No. DE-SC0017799 and Contracts No. DE-FG02-97ER41033 and No. DE-FG02-97ER41042.

[1] P. Dang, G. Riczu, and J. Cseh, Phys. Rev. C **107**, 044315 (2023).
[2] N. Anantaraman, H. Gove, J. Tōe, and H. Fortune, Phys. Lett. B **74**, 199 (1978).
[3] H. T. Fortune, A. Lacaze, and R. Sherr, Phys. Rev. C **82**, 034312 (2010).
[4] H. T. Fortune, Phys. Rev. C **68**, 034317 (2003).
[5] Z. Q. Mao, H. T. Fortune, and A. G. Lacaze, Phys. Rev. C **53**, 1197 (1996).
[6] H. T. Fortune, H. Nann, and B. H. Wildenthal, Phys. Rev. C **18**, 1563 (1978).
[7] J. Henderson, G. Hackman, P. Ruotsalainen, J. D. Holt, S. R. Stroberg, C. Andreoiu, G. C. Ball, N. Bernier, M. Bowry, R. Caballero-Folch, S. Cruz, A. Diaz Varela, L. J. Evitts, R. Frederick, A. B. Garnsworthy, M. Holl, J. Lassen, J. Measures, B. Olaizola, E. O'Sullivan *et al.*, Phys. Rev. C **105**, 034332 (2022).
[8] P. Ruotsalainen, J. Henderson, G. Hackman, G. H. Sargsyan, K. D. Launey, A. Saxena, P. C. Srivastava, S. R. Stroberg, T. Grahn, J. Pakarinen, G. C. Ball, R. Julin, P. T. Greenlees, J. Smallcombe, C. Andreoiu, N. Bernier, M. Bowry, M. Buckner, R. Caballero-Folch, A. Chester *et al.*, Phys. Rev. C **99**, 051301(R) (2019).
[9] J. Frost-Schenk, P. Adsley, A. M. Laird, R. Longland, C. Angus, C. Barton, A. Choplin, C. A. Diget, R. Hirschi, C. Marshall, F. Portillo Chaves, and K. Setoodehnia, Mon. Not. R. Astron. Soc. **514**, 2650 (2022).
[10] C. Marshall, K. Setoodehnia, K. Kowal, F. Portillo, A. E. Champagne, S. Hale, A. Dummer, and R. Longland, IEEE Trans. Instrum. Meas. **68**, 533 (2018).
[11] J. E. Spencer and H. A. Enge, Nucl. Instrum. Methods **49**, 181 (1967).
[12] F. Portillo, R. Longland, A. L. Cooper, S. Hunt, A. M. Laird, C. Marshall, and K. Setoodehnia, Phys. Rev. C **107**, 035809 (2023).
[13] M. Mayer, AIP Conf. Proc. **475**, 541 (1999).
[14] K. B. Swartz, D. W. Visser, and J. M. Baris, Nucl. Instrum. Methods Phys. Res., Sect. A **463**, 354 (2001).
[15] R. Firestone, Nucl. Data Sheets **103**, 269 (2004).
[16] I. Thompson, Comput. Phys. Rep. **7**, 167 (1988).
[17] F. Becchetti, E. Flynn, D. Hanson, and J. Sunier, Nucl. Phys. A **305**, 293 (1978).
[18] H. An and C. Cai, Phys. Rev. C **73**, 054605 (2006).
[19] M. Yahiro, Y. Iseri, H. Kameyama, M. Kamimura, and M. Kawai, Prog. Theor. Phys. Suppl. **89**, 32 (1986).
[20] R. Varner, W. Thompson, T. McAbee, E. Ludwig, and T. Clegg, Phys. Rep. **201**, 57 (1991).
[21] C. Iliadis, *Nuclear Physics of Stars* (Wiley, New York, 2008).
[22] C. Iliadis, Nucl. Phys. A **618**, 166 (1997).
[23] N. de Séréville, A. Meyer, F. Hammache, A. M. Laird, and M. Pignatari, in *Nuclear Physics in Astrophysics VIII* (NPA8 2017), edited by M. La Cognata *et al.*, EPJ Web of Conferences, Vol 165 (EDP Sciences, 2017), p. 285.
[24] A. Stanford and P. Quin, Nucl. Phys. A **342**, 283 (1980).
[25] NNDC, http://www.nndc.bnl.gov/ensdf/, 2015.
[26] C. Weldon *et al.*, Eur. Phys. J. A **26**, 321 (2005).
[27] L. L. Lee and J. P. Schiffer, Phys. Rev. Lett. **12**, 108 (1964).
[28] R. C. Johnson and F. D. Santos, Phys. Rev. Lett. **19**, 364 (1967).
[29] G. Mairle, L. K. Pao, G. Wagner, K. Knöpfle, and H. Riedesel, Z. Phys. A: At. Nucl. **301**, 157 (1981).
[30] D. C. Bailey, P. E. Carr, J. L. Durell, A. N. James, M. W. Greene, and J. F. Sharpey-Schafer, J. Phys. A: Gen. Phys. **4**, 908 (1971).
[31] A. Hoffmann, P. Betz, H. Röpke *et al.*, Z. Physik A - Atomic Nuclei **332**, 289 (1989).
[32] S. Thummerer, W. von Oertzen, T. Kokalova, H. G. Bohlen, B. Gebauer, A. Tumino, T. N. Massey, G. de Angelis, M. Axiotis, A. Gadea, T. K. ll, N. Marginean, D. R. Napoli, M. D. Poli, C. Ur, D. Bazzacco, S. M. Lenzi, C. R. Alvarez, S. Lunardi, R. Menegazzo *et al.*, J. Phys. G: Nucl. Part. Phys. **29**, 509 (2003).
[33] G. Andritsopoulos, W. Catford, E. Garman, D. Pringle, and L. Fifield, Nucl. Phys. A **372**, 281 (1981).
[34] C. Rolfs, H. Trautvetter, E. Kuhlmann, and F. Riess, Nucl. Phys. A **189**, 641 (1972).
[35] J. Hallock, H. Enge, J. Garrett, R. Middleton, and H. Fortune, Nucl. Phys. A **252**, 141 (1975).
[36] E. Kuhlmann, A. Hoffmann, and W. Albrecht, Z. Phys. **271**, 49 (1974).
[37] P. Endt, Nucl. Phys. A **521**, 1 (1990).
[38] A. Howard, J. Pronko, and C. Whitten Jr., Nucl. Phys. A **152**, 317 (1970).
[39] W. Prestwich, T. Kennett, and J.-S. Tsai, Z. Phys. A: At. Nucl. **325**, 321 (1986).
[40] E. Selin, Phys. Scr. **2**, 169 (1970).
[41] S. Hinds and R. Middleton, Proc. Phys. Soc. **74**, 779 (1959).
[42] M. Heil, R. Plag, E. Uberseder, R. Gallino, S. Bisterzo, A. Juseviciute, F. Käppeler, C. Lederer, A. Mengoni, and M. Pignatari, Phys. Rev. C **90**, 045804 (2014).
[43] R. Winters and R. Macklin, Astrophys. J. **329**, 943 (1988).
[44] M. Freer, N. Ashwood, M. Barr, N. Curtis, J. Gibelin, F. Haas, J. Malcolm, T. Munoz-Britton, G. Randisi, N. Soić *et al.*, J. Phys. G: Nucl. Part. Phys. **37**, 125102 (2010).